Eklund, Kim; Alajoki, Julia; Karttunen, Antti J.

Elastic Properties of Binary d-Metal Oxides Studied by Hybrid Density Functional Methods

Published in:
Crystal Growth and Design

DOI:
10.1021/acs.cgd.2c01543

Published: 03/05/2023

Document Version
Publisher's PDF, also known as Version of record

CRYSTAL GROWTH & DESIGN

pubs.acs.org/crystal

Article

Elastic Properties of Binary d-Metal Oxides Studied by Hybrid Density Functional Methods

Published as part of the Crystal Growth & Design virtual special issue "Lattice Dynamics".

Kim Eklund, Julia Alajoki, and Antti J. Karttunen*

Cite This: *Cryst. Growth Des.* 2023, 23, 3427−3436

Read Online

ACCESS | Metrics & More | Article Recommendations | Supporting Information

ABSTRACT: Detailed understanding of the elastic properties and mechanical durability of ceramic materials is crucial for their utilization in advanced microelectronic or micro-electromechanic devices. We have systematically investigated the elastic properties of 97 binary d-metal oxides using hybrid density functional methods. We report the polycrystalline and single-crystal bulk moduli and the symmetrized elastic constants of the studied oxides and compare the elastic properties with experimental information where available. We discuss the periodic trends of several key structure types, namely, rutile, corundum, and rocksalt, in detail. The calculated bulk moduli and elastic constants of the nonmagnetic and magnetic d-metal oxides are in reasonable overall agreement with experiment, but some materials show relatively large discrepancies between the calculated and experimental bulk moduli. In several cases, such as MnO, CoO, NiO, ReO_3, and ZrO_2 (*tP6*), some of the elastic constants calculated for ideal single crystals at 0 K are clearly different from the experimentally determined elastic constants.

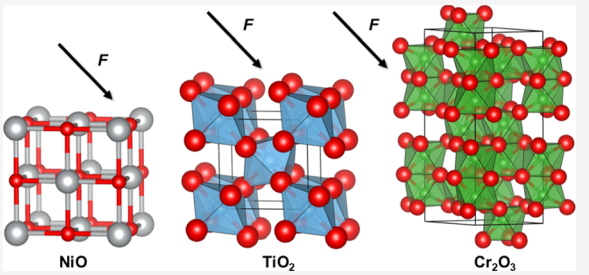

INTRODUCTION

Elastic properties of crystalline inorganic compounds provide insight into the materials' durability and strength, and many practical applications require detailed understanding of elastic properties.[1] Binary d-metal oxides are of interest for prospective applications due to their electronic, magnetic, and thermoelectric properties.[2−7] Understanding the elastic properties of d-metal oxides is thus relevant for engineering them toward new applications and devices. Elastic constants of a material are usually represented in a tensor form using Hooke's law, which constitutes a relationship between the stress and the strain and second-order elastic constants.[1,8] Crystal symmetry reduces the elastic tensor to 21 independent components that are further reduced according to the Laue class of the crystal.

The elastic constants can be measured experimentally by using several different techniques.[9] Mechanical tests can be used to find out the relation between the applied stress and strain. In dynamic techniques, the resonant frequencies of a material are measured, and a relationship between them and the elastic constant is established. Furthermore, the time-of-flight of an elastic wave in a material can be determined and used to obtain elastic constants. In addition to elastic constants, bulk modulus is a key quantity when considering the elastic properties of materials. Bulk modulus (K) represents the resistance of a material to uniform compression and is defined as the ratio of pressure change (dP) and change (dV) of volume (V), $K = -V(dP/dV)$. The bulk modulus of solids can be measured, for example, by using high-pressure X-ray diffraction and fitting the pressure and volume changes to Murnaghan's or Birch−Murnaghan's equation of state.[10−12]

Second-order elastic constants can be determined quantum chemically by studying the derivatives of total energy as a function of crystal deformation. This can be achieved either numerically or analytically, yet most current ab initio approaches are based on numerical techniques. For example, the implementation in the periodic CRYSTAL code is based on strain second derivatives obtained from analytical first derivatives of the energy for both lattice parameters and atomic positions, coupled with relaxation of atomic positions.[13] The acquired elastic compliance tensor can be used to obtain the elastic constants. From these the bulk moduli, Young's moduli, and shear moduli are acquired using the Voigt-Reuss-Hill approximation[14] and correspond to values for a polycrystalline sample. In addition to the approach of obtaining the polycrystalline bulk modulus via elastic constants, the CRYSTAL code provides an equation-of-state procedure that scans over the volume in order to compute energy versus

Received: December 29, 2022
Revised: March 21, 2023
Published: April 4, 2023

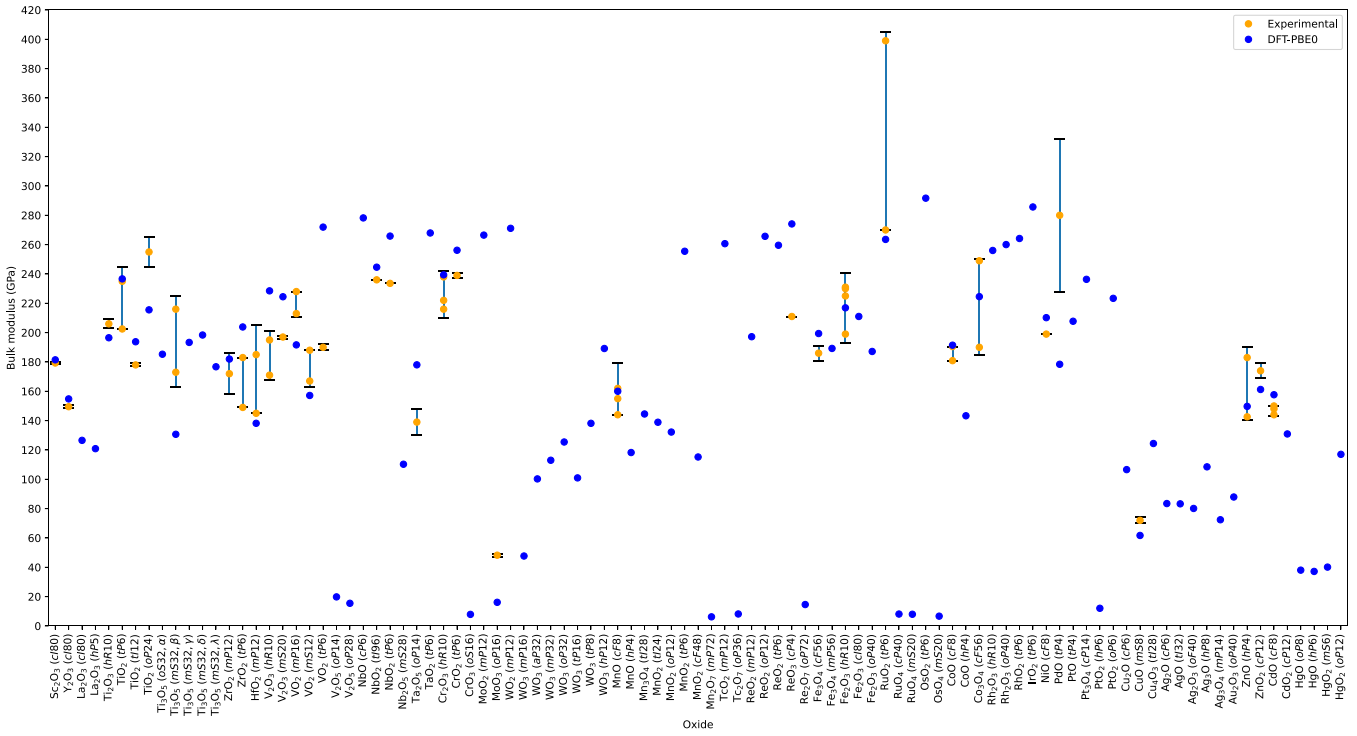

Figure 1. Bulk moduli for the studied d-metal oxides (GPa). DFT-PBE0/TZVP results in blue, experimental values in yellow (with error bars, where available). The oxides are ordered by the group of the d-metal (groups 3 to 12). References for the experimental data are in Table 1.

volume curves that are used to fit various equations of state such as Murnaghan's or Birch–Murnaghan's.[15] The equation-of-state approach, in turn, yields values of the bulk moduli corresponding to a single-crystal sample. The CRYSTAL code and hybrid density functional (DFT) methods have recently been used to study the elastic properties of highly correlated cerium oxides CeO_2 and CeO_3,[16] wurtzite-type ZnO under pressure,[17] and of various silicate garnet minerals.[18] Other recent examples of using DFT for the investigation of elastic properties include a large database of full elastic information on inorganic crystalline compounds using the VASP code.[19] Elastic properties can also be studied with many other codes such as CASTEP, ABINIT, and CP2K.[20] Typically DFT calculations of elastic properties assume a perfect crystal. While from a materials engineering point of view the presence of defects in small atomic concentrations might not be relevant, they might still affect the measurement of elastic properties when high-precision methods are used.[21] This can, in addition to temperature effects, explain some of the deviations between calculated and experimentally determined values of elastic constants.

We have recently carried out a systematic computational study on the crystal structures, magnetic ground states, and fundamental electronic properties of 100 binary d-metal oxides known at atmospheric pressure by using a hybrid DFT-PBE0 method.[22] Hybrid DFT methods generally treat the valence bands of d-metal oxide materials near the Fermi level more accurately compared to nonhybrid methods,[23] resulting in an improved description of the localization of the d electrons. Structural properties of the studied d-metal oxides were accurately described by the DFT-PBE0 method. Here we use hybrid density functional methods to investigate the elastic constants and bulk moduli of both magnetic and nonmagnetic d-metal oxides. The structure–property correlations within different structure types are investigated in detail. We systematically compare the calculated elastic properties with available experimental and computational data in the literature.

COMPUTATIONAL DETAILS

All quantum-chemical calculations have been carried out using the CRYSTAL17 program package[24] and hybrid PBE0 density functional method (DFT-PBE0, 25% exact exchange).[25,26] Localized Gaussian-type triple-ζ-valence + polarization (TZVP) basis sets, based on Karlsruhe def2 basis sets,[27] were used for all elements. All basis sets used here are available in ref 22. The same Monkhorst–Pack-type[28] k-meshes and magnetic ground states were used as in ref 22. For magnetic oxides, the space group used in the calculations might differ from the crystallographic space group, but the crystallographic space group is used here for labeling of the crystal structures. Full structural details are reported in ref 22. Tight tolerance factors (TOLINTEG) of 8, 8, 8, 8, and 16 were used for the evaluation of the Coulomb and exchange integrals (for Rh_2O_3 ($oP40$) and WO_3 ($mP16$), even tighter values of 10, 10, 10, 10, 20 had to be used). Default CRYSTAL17 geometry optimization convergence criteria and DFT integration grids were used. For RuO_2, the calculations with the larger TZVP basis set had to be carried out in space group $P1$ to avoid self-consistent field (SCF) convergence issues. The second-order elastic constants, together with bulk moduli corresponding to a Reuss model for polycrystalline samples for the optimized geometries reported in ref 22, were obtained with the fully automated procedure implemented in CRYSTAL (ELASTCON keyword).[13,15] For systems crystallizing in the rutile structure type, the elastic constants were also evaluated with an alternative scheme with an analytical evaluation of the nuclear-relaxation term using an interatomic force constant Hessian matrix (keywords NUCHESS and HESSNUM2).[29,30] Re-

https://doi.org/10.1021/acs.cgd.2c01543
Cryst. Growth Des. 2023, 23, 3427–3436

ported elastic properties have been obtained for three points and a second-order fit. Bulk moduli were also calculated with the equation-of-state (EOS) fitting approach implemented in CRYSTAL[15] to obtain values corresponding to experimental single-crystal measurements. The default settings of CRYSTAL17 were used for the EOS calculations (unit cell volume range ±8%). For some materials, the EOS calculations had to be carried out with reduced range (unit cell volume range ±5%) to avoid SCF convergence issues, and in some cases TOLINTEG had to be increased to 10 10 10 10 20, and the geometry was reoptimized before the EOS calculation. These calculations were carried out with CRYSTAL23.[31] Full technical details for all elastic property calculations are openly available as CRYSTAL output files at a Github repository.[32] Nonstochiometric rutile-type oxide TaO_2 not previously reported in ref 22 was also included, the calculations being performed with a *k*-mesh of 8 × 8 × 12.

RESULTS

We studied the elastic properties of almost all d-metal oxides studied in ref 22. TiO (*hP6*) was not included in this study due to its nonstoichiometry. Mn_2O_3 (*cI80*) and Mn_2O_3 (*oP80*), which are effectively the same structure with different magnetic ordering, were not included due to technical problems with elastic constant calculations on the fairly large unit cells with complex magnetic ordering.

We first discuss the calculated bulk moduli and investigate periodic trends within structure types important for d-metal oxides. In the case of second-order elastic constants, we focus on comparisons with available experimental data. The full elastic tensors for the studied materials are available as Supporting Information (as CRYSTAL output files).[32] The densities of the optimized structures were also employed in the analysis of the elastic properties and are included as Supporting Information.

Bulk Moduli. The DFT-PBE0/TZVP bulk moduli of all the studied compounds along with the available experimental data are presented in Figure 1 and Table 1. The reported calculated bulk moduli correspond to the Reuss model. Bulk moduli of some binary d-metal oxides have also been reported in previous computational studies, but here we focus on comparisons to experimental bulk moduli (see, e.g., TiO_2,[33] NiO,[34] and other d-metal monoxides[35]).

As expected, molecular crystals with weak intermolecular interactions between the molecular units possess the smallest bulk moduli of the studied oxides. For example, the bulk moduli of CrO_3 (*oS16*), Mn_2O_7 (*mP72*), and OsO_4 (*mS20*) are only 8, 6, and 7 GPa, respectively. When considerng nonmolecular oxides, the smallest bulk moduli of 3d, 4d, and 5d oxides are found for layer-structured oxides V_2O_5 (*oP28*), MoO_3 (*oP16*), and PtO_2 (*hP6*), with values of 15, 16, and 12 GPa, respectively. If the layer-structured oxides are excluded, the smallest bulk moduli of 3d, 4d, and 5d oxides are obtained for CuO (*mS8*), Ag_3O_4 (*mP14*), and HgO (*hP6*), with values of 62, 72, and 37 GPa, respectively. All binary mercury oxides show remarkably small bulk moduli values. For HgO_2 (*mS6*) and HgO_2 (*oP12*), large errors of about 30% and 10%, respectively, compared to experimental lattice parameter values were observed upon geometry optimization.[22] Some of the largest values of bulk moduli are found for rutile-structured oxides. The largest bulk moduli by period are found for VO_2 (*tP6*), NbO (*cP6*), and OsO_2 (*tP6*), with bulk moduli of 277, 276, and 292 GPa, respectively.

Table 1. DFT-PBE0/TZVP Bulk Moduli for d-Metal Oxides with Reported Experimental Data (GPa)[a]

Oxide	DFT	Experimental values
Sc_2O_3 *cI80*	181	179.3 ± 1[36]
Ti_2O_3 *hR10*	197	206 ± 3[37]
TiO_2 *tP6*	237	202.5,[38] 235 ± 10[39]
TiO_2 *tI12*	194	178 ± 2[40]
TiO_2 *oP24*	216	255 ± 10[41]
β-Ti_3O_5 *mS32*	131	216 ± 9,[42] 173 ± 10[43]
V_2O_3 *hR10*	228	195 ± 6,[44] 171 ± 3[45]
V_2O_3 *mS20*	224	197 ± 1[46]
VO_2 *mP16*	192	228,[47] 213 ± 2[48]
VO_2 *mS12*	157	188,[47] 167 ± 4[48]
VO_2 *tP6*	272	190 ± 2[48]
Cr_2O_3 *hR10*	239	216 ± 6,[49] 231 ± 5,[45] 238 ± 4[44]
CrO_2 *tP6*	256	239 ± 2[50]
MnO *cF8*	160	144,[12] 155,[51] 144[52] 162 ± 17[53]
Fe_3O_4 *cF56*	199	186 ± 5[54]
Fe_2O_3 *hR10*	217	231 ± 10,[45] 225 ± 4,[44] 199 ± 6,[55] 230 ± 5[56]
CoO *cF8*	191	180.9,[57] 190.5[12]
Co_3O_4 *cF56*	225	190 ± 5,[58] 249 ± 1[59]
NiO *cF8*	210	199[12]
Cu_2O *cP6*	107	112[60]
CuO *mS8*	62	72 ± 2[61]
Y_2O_3 *cI80*	155	149.5 ± 1[62]
ZrO_2 *mP12*	182	172[63]
ZrO_2 *tP6*	204	149[64]
NbO_2 *tI96*	245	236 ± 6[65]
NbO_2 *tP6*	266	233.6[66]
MoO_3 *oP16*	16	48.25 ± 1[67]
RuO_2 *tP6*	264	399 ± 6,[68] 270[69]
PdO *tP4*	178	280 ± 52[70]
CdO *cF8*	158	147 ± 4,[71] 148−150[52]
HfO_2 *mP12*	138	185 ± 20,[72] 145[73]
ReO_3 *cP4*	274	211[74]

[a]The oxides are ordered according to periodic rows (3d, 4d, and 5d).

The bulk moduli for the rutile, distorted rutile, corundum, and rocksalt structure types are discussed in detail below due to interest in these structure types and abundance of experimental data. A comprehensive list of all calculated bulk moduli of the investigated oxides is given in the Supporting Information.

Rutile and Distorted Rutile Structure Types. Rutile is the thermodynamically most stable polymorph of TiO_2 and gives its name to the rutile-type structure of AB_2 oxides and fluorides in the tetragonal space group $P4_2/mnm$.[75] Distorted versions of the rutile structure type are also common for d-metal oxides such as MoO_2 or WO_2.[76] Typically, in this distortion, the metal atoms appear in pairs along the *c* axis of the rutile pseudocell, and the resulting structures belong to monoclinic space groups ($P2_1/c$ for MoO_2-type). Of these rutile-structured oxides, IrO_2, RuO_2, and RhO_2 show metallic character.[77,78]

In addition to exhibiting the highest bulk moduli of the oxides investigated here, the rutile structure type is characterized by high anisotropic compressibility with the *a* axis experimentally observed to be approximately twice as compressible as *c*.[69] While both the prototypical rutile (*tP6*) and anatase (*tI12*) polymorphs of TiO_2 consist of TiO_6

https://doi.org/10.1021/acs.cgd.2c01543
Cryst. Growth Des. 2023, 23, 3427−3436

octahedra, the packing is different, explaining the higher bulk modulus and compressible anisotropy of rutile.[33] In rutile, the octahedra share edges along the *c* direction and corners along the *ab* planes. Corners share just one Ti−O bond while edges share two, making the *c* direction more compressible. In anatase, the octahedra are arranged in a zigzag motif with the sharing of four edges, but the edges do not lie at opposite ends like in rutile, allowing for more uniform compressibility of the structure.

The calculated and experimental values of the bulk moduli for rutile-type oxides are summarized in Figure 2. A general

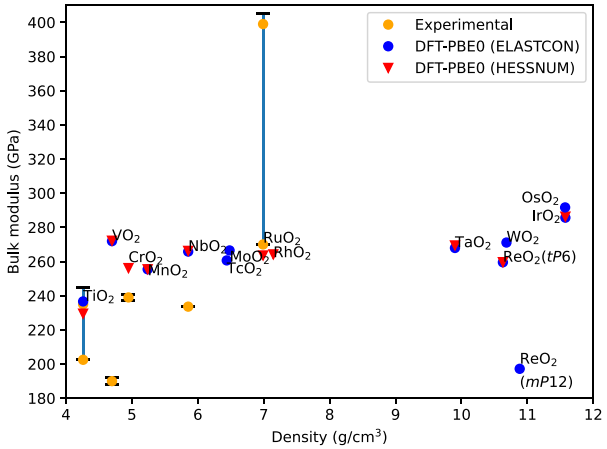

Figure 2. Bulk moduli of the studied rutile and distorted rutile-type d-metal oxides as a function of density. Values calculated (DFT-PBE0) with the ELASTCON approach in blue circles, values calculated with NUCHESS+HESSNUM approach in red triangles, and experimental values with error bars in yellow circles and blue lines.

trend of the bulk moduli slightly increasing with the density is observed both experimentally and in our computational results. Likewise, an increase in the bulk moduli is associated with the increasing value of the Pauling electronegativity of the d-metal for corresponding oxides (see Supporting Information, Figure S1). For ReO_2, both a distorted rutile (MoO_2-type, *mP*12) and a rutile structure (*tP*6) are reported.[79,80] In our geometry optimization we observed a large difference of about 14% for the lattice constant *c* of rutile-type ReO_2 (*tP*6).[22] However, despite this, the rutile-type structure shows a similar bulk modulus compared to the other rutile and distorted rutile structures. The distorted rutile polymorph of ReO_2 exhibits a smaller bulk modulus than the other similar oxides.

Rutile-type VO_2 existing at elevated temperatures has been experimentally found to be metallic, while our calculations yield a band gap of 2.8 eV.[22] This could indicate non-stoichiometry, which would explain the larger discrepancy between the experimental and calculated value of the bulk modulus.

In order to compare the two implemented approaches for calculation of elastic properties in CRYSTAL, the NUCHESS approach was tested for all the rutile-structured oxides that crystallize in the ideal $P4_2/mnm$ space group (see Computational Details). The initial reason for this test was that the standard ELASTCON approach failed for CrO_2, RhO_2, and RuO_2. For VO_2, MnO_2, IrO_2, TaO_2, and ReO_2 the values of the two different approaches are effectively the same, but for TiO_2, the NUCHESS method yielded a value of 230 GPa that is 7 GPa smaller compared to the standard approach.

Corundum Structure Type. The corundum-type structures of d-metal oxides in trigonal space group $R\bar{3}c$ derive their name from the structure of Al_2O_3.[81] Ti_2O_3, V_2O_3, Cr_2O_3, Rh_2O_3, and α-Fe_2O_3 crystallize in the corundum structure type. For Ti_2O_3, we previously observed an imaginary frequency upon harmonic frequency calculations,[22] and the structure ($C1c1$) resulting from subsequent distortion along the imaginary mode has been used for the calculation of elastic properties.

The calculated and experimental values are summarized in Figure 3. Like for rutile-structured oxides, the increase of the d-

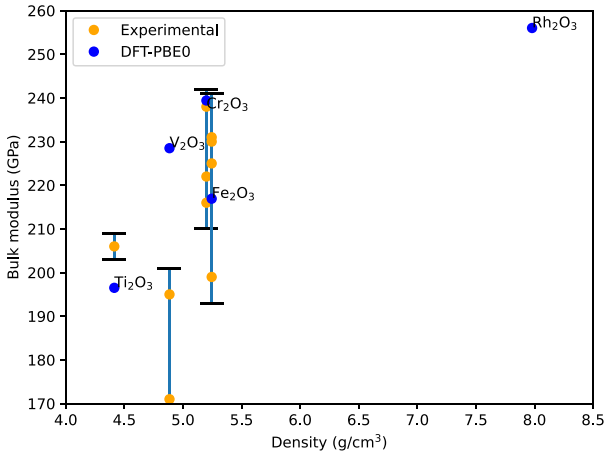

Figure 3. Bulk moduli of the studied corundum-type d-metal oxides as a function of density. Calculated DFT-PBE0 values in blue and experimental values with error limits in yellow.

metal Pauling electronegativity generally coincides with an increase of the bulk modulus of the oxide (see Supporting Information, Figure S2), albeit for Fe_2O_3 this value is clearly below the trend of other 3d oxides. Unlike observations in the experimental measurements of Sato et al.,[45] the bulk modulus of V_2O_3 is not noticeably smaller compared to other corundum-structured oxides. Instead, the value for Ti_2O_3 is smaller, likely due to the further lowering of the symmetry due to the magnetic configuration and distortion along the imaginary mode. This smaller value is also observed experimentally.[37]

The bulk modulus of corundum-structured Rh_2O_3 has previously been reported to be smaller by about 1 GPa than that of rutile-structured RhO_2 at the DFT-PBE/FPLAPW level of theory.[82] This is also corroborated by our results, with the difference being 8 GPa and bulk modulus values of Rh_2O_3 and RhO_2 being 256 and 264 GPa, respectively.

Rocksalt Structure Type. The cubic rocksalt structure type ($Fm\bar{3}m$) derives its name from NaCl and is adopted by a number of d-metal oxides with divalent metal cations; MnO, CoO, NiO, and CdO.[83] FeO would also adopt a similar structure, but it is excluded in our studies due to nonstoichiometry.

The calculated and experimental values are summarized in Figure 4. The antiferromagnetic ordering of MnO, CoO, and NiO lowers the space group from cubic to trigonal in the calculations, but the values of the bulk moduli are in reasonable agreement with the experimental values. For the nonmagnetic oxide CdO, a good agreement is also observed. Our reported values have a trend of being larger than previously reported values at the DFT-PBE0/FP-(L)APW+lo level of theory (143 GPa for MnO, 167 GPa for CoO, and 187

https://doi.org/10.1021/acs.cgd.2c01543
Cryst. Growth Des. 2023, 23, 3427−3436

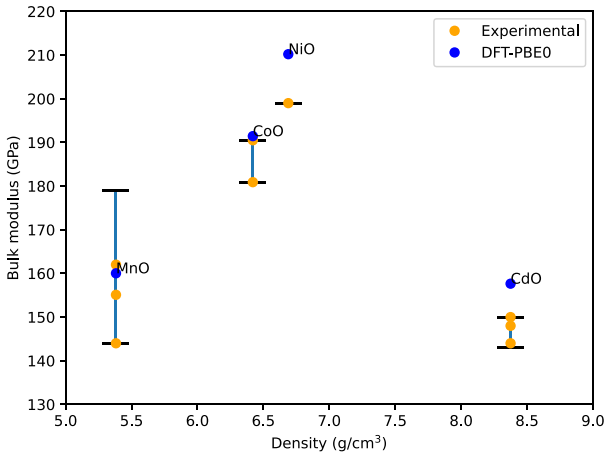

Figure 4. Bulk moduli of the studied rocksalt-type d-metal oxides as a function of density. Calculated DFT-PBE0 values in blue and experimental values with error limits in yellow.

GPa for NiO)[35] but offer a slightly better agreement with the experimental results. For CdO, the reported calculated value is almost identical to the previously reported DFT-LDA computational value of 158 GPa.[84] The difference in bulk moduli of the 3d rocksalt oxides and 4d CdO has previously been attributed to the increased electronegativity compared to ionic radius in CdO.[52]

Polycrystalline Versus Monocrystalline Bulk Moduli. In order to compare the difference between polycrystalline and monocrystalline bulk moduli, we also calculated monocrystalline bulk moduli using the Birch−Murnaghan equation-of-state (EOS). The unit cell volume changes included in the EOS procedure resulted in serious SCF convergence issues for some of the studied metal oxides, especially metallic rutile-type oxides. In the end, we were able to obtain monocrystalline bulk moduli for 86 d-metal oxides. The data are listed in the Supporting Information (Tables S1−S3), and both the polycrystalline and monocrystalline bulk moduli are compared to experimental bulk moduli in Figure S4. For most of the studied materials, the differences of the polycrystalline and monocrystalline bulk moduli are small (0−2%), but larger differences of more than 5% were obtained for some triclinic, monoclinic, and orthorhombic oxides such as ZrO_2 (*mP*12) with 6% difference. The largest deviations were obtained for the polymorphs of WO_3, especially for *oP*32 (+22%).

Elastic Constants and Moduli. Symmetrized elastic constants and elastic moduli compliance tensors were also obtained for all the structures discussed above. As experimental data is scarcer than for bulk moduli, the results here introduce just a few selected oxides for which experimental information could be found. Full elastic constants and compliance tensors of all investigated oxides are given in the associated GitHub repository.[32] While computational studies have also been performed with DFT for a number of d-metal oxides including ZrO_2,[85] ZnO,[86] and Cu_2O,[87] we discuss here only oxides for which the experimental values of elastic constants are available.

Rutile TiO_2. The calculated and experimental values of the elastic constants of rutile-type TiO_2 are presented in Table 2. The calculated values are generally larger than the experimental ones, with C_{33} showing the largest difference. However, the experimental values also vary quite considerably. Employing a DFT-PBE approach, Iuga et al. report a better fit with the experimental values, especially for C_{33}.[88] Our C_{33} value is roughly 1.8 times larger than C_{11}, corresponding with the observation of Hazen et al.[69] that, for rutile-type oxides, the *a* axis is close to twice more compressible than the *c* axis. The ratio is similar for some rutile-type oxides such as OsO_2 (1.9) and RhO_2 (1.8) but notably lower for CrO_2 (1.2), TaO_2 (1.2), and NbO_2 (1.1).

Table 2. Elastic Constants of Rutile TiO_2 (*tP*6)

	DFT (this work)	Exp[89]	Exp[90]	Exp[38]	DFT-PBE[88]
C_{11}	300	273	248 ± 8	266 ± 7	278
C_{33}	528	484	452 ± 8	470 ± 8	479
C_{44}	129	125	120 ± 3	124 ± 7	115
C_{66}	243	194	160 ± 10	189 ± 5	214
C_{12}	200	176	200 ± 10	173 ± 7	153
C_{13}	174	149	140 ± 10	136 ± 8	149

Harmonic frequency calculations for TiO_2 at the PBE0-TZVP level of theory yield an imaginary vibration of 76*i* cm^{-1}. It is well-known that with DFT despite of Hamiltonian choice the anatase phase is found to be more stable than rutile, while experimental studies indicate the opposite.[91] Despite this instability indicated by frequency calculations, the calculated elastic constants indicate that rutile TiO_2 is mechanically stable since the Born stability criteria are satisfied $C_{11} > |C_{12}|$, $2C_{13} < C_{33}(C_{11} + C_{12})$, $C_{44} > 0$, $C_{66} > 0$.[92]

Wurtzite-type ZnO. Zinc oxide ZnO exists in the hexagonal wurtzite and cubic zinc blende structures,[86,93] of which the wurtzite polymorph is thermodynamically more stable. The structure type is also adopted by various semiconductor materials such as GaN. The calculated elastic constants of wurtzite-type ZnO, presented in Table 3, show good agreement with measured values for both bulk[94] and thin-film samples.[95] Our values are also comparable with the previous results obtained with DFPT[93,96] and DFT-LDA.[86] The nonindependent C_{66} constant, defined as $(C_{11} - C_{12})/2$, is usually hard to determine experimentally.[95]

Table 3. Elastic Constants of Wurtzite-type ZnO (*hP*4)[a]

	DFT (this work)	Exp[94]	Exp[95]	DFPT-LDA[93]	DFPT-GGA+U[96]	DFT-LDA[86]
C_{11}	218	209	206 ± 4	220	203	217
C_{12}	131	120		139	110	117
C_{13}	111	104.4	118 ± 10	124	92	121
C_{33}	212	216	211 ± 4	243	210	225
C_{44}	43.2	44.2	44.3 ± 1	38	43	50
C_{66}	43.5	44.2	44.6 ± 1			

[a]For a hexagonal crystal system, $C_{66} = (C_{11} - C_{12})/2$.

Zirconia ZrO_2. Zirconia ZrO_2 is a material of interest due to its optimal mechanical, chemical, and dielectric properties.[85] It also exhibits considerable polymorphism under temperature and pressure variations. The room-temperature polymorph is monoclinic. The elastic tensor of monoclinic zirconium oxide takes a more complex form due to the low symmetry of the compound in the $P2_1/c$ (14) space group. The calculated and experimental values tabulated in Table 4 are in good agreement for the diagonal elements (C_{11} to C_{66}), but some of the other constants, such as C_{15} and C_{25}, show larger discrepancies. Similar performance is observed with DFT-PBE/PAW by Fadda et al.[85]

Rocksalt Structure Type. Cubic symmetry limits the number of experimentally measurable elastic moduli compo-

https://doi.org/10.1021/acs.cgd.2c01543
Cryst. Growth Des. 2023, 23, 3427−3436

Table 4. Elastic Constants of Monoclinic ZrO_2 (*mP*12)

	DFT (this work)	Exp[97]	Exp[63]	DFT-PBE[85]
C_{11}	331	358	361	337
C_{12}	176	144	142	155
C_{13}	93	67.0	55.0	84
C_{15}	48	−25.9	−21.3	26
C_{22}	415	426	408	351
C_{23}	159	127	196	153
C_{25}	−4	38.3	31.2	−4
C_{33}	260	240	258	268
C_{35}	13	−23.3	−18.2	2
C_{44}	98	99.1	99.9	79
C_{46}	−11	−38.8	−22.7	−15
C_{55}	96	78.7	81.2	70
C_{66}	138	130	126	114

nents to three, C_{11}, C_{12}, and C_{44}.[98] For antiferromagnetic MnO, NiO, and CoO calculations have been carried out in the trigonal space group $R\bar{3}m$ to reproduce the antiferromagnetic ordering. Due to this lowering of symmetry from the cubic symmetry in space group $Fm\bar{3}m$, the elastic constants and moduli cannot be directly compared with experimental data.

To compare the calculated and experimental elastic moduli components we utilized a projection method previously utilized for $Ti_{0.5}Al_{0.5}N$ and CrN[99,100] to average elastic moduli components C_{11}, C_{12}, and C_{44}, which we report here according to cubic symmetry as $\bar{C}_{11} = (C_{11} + C_{22} + C_{33})/3$, $\bar{C}_{12} = (C_{12} + C_{13} + C_{23})/3$, and $\bar{C}_{44} = (C_{44} + C_{55} + C_{66})/3$. The calculated and experimental values are tabulated in Table 5. The full elastic moduli components in the trigonal symmetry are available in the Supporing Information (Table S4).

Despite the symmetry breaking, the bulk moduli of the studied cubic oxides show a good agreement with the experimental data. It is notable that there is an increasing trend in the bulk moduli and elastic moduli components when moving along the periodic row from MnO to NiO, observable both in the experimental and calculated elements. Like in the bulk modulus, the elastic tensor component values for 4d oxide CdO is smaller than for the antiferromagnetic 3d oxides. Even with averaging, the DFT-PBE0 values of the elastic moduli component C_{11} remain higher than the experimentally measured ones, for MnO, CoO, and NiO. A similar trend was reported in a recent study with the DFT-PBEsol functional, where the C_{11} elastic constants of NiO and CoO were overestimated compared to the experimental values.[101] A previous DFT study on antiferromagnetic refractory material CrN reported the elastic constants of the magnetically ordered system to be overestimated compared to experimental values and the values obtained for a paramagnetic model system.[100]

Other Cubic and Tetragonal Oxides. Finally, we present the elastic constants calculated for other cubic and tetragonal oxides, for which experimental data are available. The calculated and experimentally determined elastic constants of the cubic rhenium(VI) oxide ReO_3, yttria Y_2O_3, and copper(I) oxide Cu_2O are given in Table 6. The calculated and experimental values for Y_2O_3 and Cu_2O are in reasonable agreement, although the C_{11} values are overestimated in comparison to the experimental values.

Table 6. Calculated (DFT-PBE0) and Experimental Elastic Constants of Y_2O_3 (*cI*80), Cu_2O (*cP*6), and ReO_3 (*cP*4)

	Y_2O_3 DFT	Y_2O_3 Exp[62]	Cu_2O DFT	Cu_2O Exp[104]	ReO_3 DFT	ReO_3 Exp[74]
C_{11}	234	224	155	122.88	701	517.8
C_{12}	115	112	102	106.50	61	7
C_{44}	81	75	12	12.10	77	68.06

For ReO_3, the calculated and experimental values of C_{11} and C_{12} differ considerably: the calculated C_{11} is 701 GPa, while the experimentally determined value of 517.8 GPa is clearly smaller. The value of the bulk modulus for ReO_3 differs as well (274 GPa DFT-PBE0 vs 211 GPa experimental[74]). ReO_3 is a highly anisotropic material also according to experimental measurements, and the experimental anisotropy factor $A = 2C_{44}/(C_{11} - C_{12}) = 0.24$ is also reproduced in our calculations, even though the calculated value of C_{12} is larger the experimentally observed one.

The calculated and experimentally determined elastic constants of the tetragonal modifications of NbO_2 and ZrO_2 are given in Table 7. The calculated and experimental values for NbO_2 are in reasonable agreement, but for ZrO_2 the calculated values are clearly overestimated in comparison to experiment. Our calculated bulk modulus of ZrO_2 is also over 50 GPa larger than experimentally determined.

Table 7. Calculated (DFT-PBE0) and Experimental Elastic Constants of NbO_2 (*tI*96) and ZrO_2 (*tP*6)

	NbO_2 DFT	NbO_2 Exp[65]	ZrO_2 DFT	ZrO_2 Exp[64]
C_{11}	458	433	410	327
C_{12}	83	93	230	100
C_{13}	175	171	70	62
C_{16}	0.1		0	
C_{26}	−0.1		0	
C_{33}	431	388	359	264
C_{44}	94	94	63	59
C_{66}	59	57	198	64

Table 5. Calculated (DFT-PBE0) and Experimental Elastic Constants of Rocksalt-type Oxides MnO ($R\bar{3}m$), CoO ($R\bar{3}m$), NiO ($R\bar{3}m$), and CdO ($Fm\bar{3}m$)[a]

	MnO DFT	MnO Exp[98]	MnO Exp[102]	CoO DFT	CoO Exp[98]	NiO DFT	NiO Exp[98]	NiO Exp[103]	CdO DFT
C_{11}	270	223	222	305	255.6	352	270	225	246
C_{12}	106	120	109.9	135	143.6	139	125	95	114
C_{44}	75	79	78.6	96	80.3	127	105	110	62

[a]For antiferromagnetic MnO, CoO, and NiO the calculated elastic moduli of the trigonal magnetic structure have been averaged for comparison with measurements in the cubic symmetry.

https://doi.org/10.1021/acs.cgd.2c01543
Cryst. Growth Des. 2023, 23, 3427−3436

CONCLUSION

We investigated the elastic properties of almost all binary d-metal oxides known at ambient pressure. The DFT-PBE0/TZVP level of theory has previously been shown to describe the structural parameters of magnetic d-metal oxides with good accuracy, and for elastic properties the overall agreement with experiment is also at a reasonable level. However, in several cases there are relatively large discrepancies between the calculated and experimental bulk moduli and elastic constants. The calculated bulk moduli and elastic constants are for ideal perfect crystals at 0 K, not taking into account defects or temperature effects. More extensive comparisons between the experimental and calculated data are also complicated by the variance of the experimental data and measurement conditions. Especially for high-temperature applications, it is necessary to also take into account temperature effects, as demonstrated for refractory materials such as CrN[100] and TiN.[105] The elastic properties of ordered 0 K ground state can clearly differ from the elastic properties of higher-temperature paramagnetic ground state. Overall, the elastic properties of both nonmagnetic and magnetic d-metal oxides can be studied systematically with hybrid DFT methods, but in many cases, methodological improvements are required to reach a quantitative agreement with experimentally determined elastic constants. In line with a previous study focusing on cubic nonoxide semiconductors and insulators, the C_{11} elastic constants, in particular, are overestimated by DFT-PBE0 in comparison to experimental values.[106] Possible routes toward improvement are the incorporation of defects such as nonstoichiometry in the structural models and considering the effect of phonon anharmonicity and finite temperature, especially for magnetic oxides where the elastic constants have been measured for a paramagnetic ground state.

ASSOCIATED CONTENT

Supporting Information

The Supporting Information is available free of charge at https://pubs.acs.org/doi/10.1021/acs.cgd.2c01543.

Calculated (DFT-PBE0) single-crystal and polycrystalline bulk moduli, polycrystalline elastic properties, and densities of studied binary d-metal oxides. Calculated (DFT-PBE0) elastic moduli components of rocksalt-type oxides MnO, CoO, and NiO in the antiferromagnetic ground state (trigonal crystal system). Calculated (DFT-PBE0) bulk moduli of the studied rutile, distorted rutile, and corundum-type oxides versus the Pauling electronegativity of the d-metal. Calculated (DFT-PBE0) and experimental bulk moduli and densities of the studied oxide. Bulk moduli calculated with both ELASTCON (polycrystalline) and EOS (single crystal) approaches, compared with experimental bulk moduli. Full CRYSTAL outputs of the ELASTCON and EOS calculations (GitHub repository, link provided in the main paper) (PDF)

AUTHOR INFORMATION

Corresponding Author

Antti J. Karttunen − *Department of Chemistry and Materials Science, Aalto University, FI-00076 Aalto, Finland;* orcid.org/0000-0003-4187-5447; Email: antti.karttunen@aalto.fi

Authors

Kim Eklund − *Department of Chemistry and Materials Science, Aalto University, FI-00076 Aalto, Finland*

Julia Alajoki − *Department of Chemistry and Materials Science, Aalto University, FI-00076 Aalto, Finland*

Complete contact information is available at: https://pubs.acs.org/10.1021/acs.cgd.2c01543

Notes

The authors declare no competing financial interest.

ACKNOWLEDGMENTS

This research was funded by the Academy of Finland, Grant No. 317273. We thank CSC, the Finnish IT Center for Science for computational resources.

REFERENCES

(1) Nye, J. F. *Physical properties of crystals: their representation by tensors and matrices;* Clarendon: Oxford, England, 1957; p 322.

(2) Rao, C. N. R. Transition Metal Oxides. *Annu. Rev. Phys. Chem.* **1989**, *40*, 291−326.

(3) Lany, S. Semiconducting transition metal oxides. *J. Phys.: Condens. Matter* **2015**, *27*, 283203.

(4) Kieslich, G.; Cerretti, G.; Veremchuk, I.; Hermann, R. P.; Panthöfer, M.; Grin, J.; Tremel, W. A chemists view: Metal oxides with adaptive structures for thermoelectric applications. *Phys. Status Solidi A* **2016**, *213*, 808−823.

(5) Védrine, J. C. Metal Oxides in Heterogeneous Oxidation Catalysis: State of the Art and Challenges for a More Sustainable World. *ChemSusChem* **2019**, *12*, 577−588.

(6) Walia, S.; Balendhran, S.; Nili, H.; Zhuiykov, S.; Rosengarten, G.; Wang, Q. H.; Bhaskaran, M.; Sriram, S.; Strano, M. S.; Kalantar-zadeh, K. Transition metal oxides − Thermoelectric properties. *Prog. Mater. Sci.* **2013**, *58*, 1443−1489.

(7) Zhu, Y.; Lin, Q.; Zhong, Y.; Tahini, H. A.; Shao, Z.; Wang, H. Metal oxide-based materials as an emerging family of hydrogen evolution electrocatalysts. *Energy Environ. Sci.* **2020**, *13*, 3361−3392.

(8) Barron, T. H. K.; Klein, M. L. Second-order elastic constants of a solid under stress. *Proc. Phys. Soc.* **1965**, *85*, 523−532.

(9) Czichos, H.; Saito, T.; Smith, L. *Springer Handbook of Materials Measurement Methods;* Springer: Berlin, Germany, 2007; p 1207.

(10) Murnaghan, F. D. The Compressibility of Media under Extreme Pressures. *Proc. Natl. Acad. Sci. U.S.A.* **1944**, *30*, 244−247.

(11) Birch, F. Finite Elastic Strain of Cubic Crystals. *Phys. Rev.* **1947**, *71*, 809−824.

(12) Clendenen, R. L.; Drickamer, H. G. Lattice Parameters of Nine Oxides and Sulfides as a Function of Pressure. *J. Chem. Phys.* **1966**, *44*, 4223−4228.

(13) Perger, W.; Criswell, J.; Civalleri, B.; Dovesi, R. Ab-initio calculation of elastic constants of crystalline systems with the CRYSTAL code. *Comput. Phys. Commun.* **2009**, *180*, 1753−1759.

(14) Chung, D. H.; Buessem, W. R. The Voigt-Reuss-Hill Approximation and Elastic Moduli of Polycrystalline MgO, CaF_2, β-ZnS, ZnSe, and CdTe. *J. Appl. Phys.* **1967**, *38*, 2535−2540.

(15) Erba, A.; Mahmoud, A.; Orlando, R.; Dovesi, R. Elastic properties of six silicate garnet end members from accurate ab initio simulations. *Phys. Chem. Miner.* **2014**, *41*, 151−160.

(16) Brugnoli, L.; Ferrari, A. M.; Civalleri, B.; Pedone, A.; Menziani, M. C. Assessment of Density Functional Approximations for Highly Correlated Oxides: The Case of CeO_2 and Ce_2O_3. *J. Chem. Theory Comput.* **2018**, *14*, 4914−4927.

(17) Marana, N. L.; Casassa, S. M.; Sambrano, J. R. Piezoelectric, elastic, Infrared and Raman behavior of ZnO wurtzite under pressure from periodic DFT calculations. *Chem. Phys.* **2017**, *485−486*, 98−107.

(18) Erba, A.; Mahmoud, A.; Belmonte, D.; Dovesi, R. High pressure elastic properties of minerals from ab initio simulations: The

case of pyrope, grossular and andradite silicate garnets. *J. Chem. Phys.* **2014**, *140*, 124703.
(19) de Jong, M.; Chen, W.; Angsten, T.; Jain, A.; Notestine, R.; Gamst, A.; Sluiter, M.; Krishna Ande, C.; van der Zwaag, S.; Plata, J. J; Toher, C.; Curtarolo, S.; Ceder, G.; Persson, K. A.; Asta, M.; et al. Charting the complete elastic properties of inorganic crystalline compounds. *Sci. Data* **2015**, *2*, 150009.
(20) Kiely, E.; Zwane, R.; Fox, R.; Reilly, A. M.; Guerin, S. Density functional theory predictions of the mechanical properties of crystalline materials. *CrystEngComm* **2021**, *23*, 5697−5710.
(21) Hoagland, R. G.; Fensin, S. J. Signatures of the effects of defects on the bulk moduli of crystalline solids. *Comput. Mater. Sci.* **2021**, *198*, 110705.
(22) Kuklin, M. S.; Eklund, K.; Linnera, J.; Ropponen, A.; Tolvanen, N.; Karttunen, A. J. Structural Properties and Magnetic Ground States of 100 Binary d-Metal Oxides Studied by Hybrid Density Functional Methods. *Molecules* **2022**, *27*, 874.
(23) Østrøm, I.; Hossain, M. A.; Burr, P. A.; Hart, J. N.; Hoex, B. Designing 3d metal oxides: selecting optimal density functionals for strongly correlated materials. *Phys. Chem. Chem. Phys.* **2022**, *24*, 14119−14139.
(24) Dovesi, R.; Erba, A.; Orlando, R.; Zicovich-Wilson, C. M.; Civalleri, B.; Maschio, L.; Rérat, M.; Casassa, S.; Baima, J.; Salustro, S.; Kirtman, B. Quantum-mechanical condensed matter simulations with CRYSTAL. *Wiley Interdiscip. Rev. Comput. Mol. Sci.* **2018**, *8*, e1360.
(25) Perdew, J. P.; Burke, K.; Ernzerhof, M. Generalized Gradient Approximation Made Simple. *Phys. Rev. Lett.* **1996**, *77*, 3865−3868.
(26) Adamo, C.; Barone, V. Toward reliable density functional methods without adjustable parameters: The PBE0 model. *J. Chem. Phys.* **1999**, *110*, 6158−6170.
(27) Weigend, F.; Ahlrichs, R. Balanced basis sets of split valence, triple zeta valence and quadruple zeta valence quality for H to Rn: Design and assessment of accuracy. *Phys. Chem. Chem. Phys.* **2005**, *7*, 3297−3305.
(28) Monkhorst, H. J.; Pack, J. D. Special points for Brillouin-zone integrations. *Phys. Rev. B* **1976**, *13*, 5188−5192.
(29) Erba, A. The internal-strain tensor of crystals for nuclear-relaxed elastic and piezoelectric constants: on the full exploitation of its symmetry features. *Phys. Chem. Chem. Phys.* **2016**, *18*, 13984−13992.
(30) Erba, A.; Caglioti, D.; Zicovich-Wilson, C. M.; Dovesi, R. Nuclear-relaxed elastic and piezoelectric constants of materials: Computational aspects of two quantum-mechanical approaches. *J. Comput. Chem.* **2017**, *38*, 257−264.
(31) Erba, A.; Desmarais, J. K.; Casassa, S.; Civalleri, B.; Donà, L.; Bush, I. J.; Searle, B.; Maschio, L.; Edith-Daga, L.; Cossard, A.; Ribaldone, C.; Ascrizzi, E.; Marana, N. L.; Flament, J.-P.; Kirtman, B. CRYSTAL23: A Program for Computational Solid State Physics and Chemistry. *J. Chem. Theor. Comput.*. **2022**, *XXX*, XXX-XXX. DOI: 10.1021/acs.jctc.2c00958
(32) Binary d-metal oxides, *Github* repository. https://github.com/aalto-imm/d-oxides.
(33) Muscat, J.; Swamy, V.; Harrison, N. M. First-principles calculations of the phase stability of TiO_2. *Phys. Rev. B* **2002**, *65*, 224112.
(34) Mitra, C.; Krogel, J. T.; Santana, J. A.; Reboredo, F. A. Many-body ab initio diffusion quantum Monte Carlo applied to the strongly correlated oxide NiO. *J. Chem. Phys.* **2015**, *143*, 164710.
(35) Tran, F.; Blaha, P.; Schwarz, K.; Novák, P. Hybrid exchange-correlation energy functionals for strongly correlated electrons: Applications to transition-metal monoxides. *Phys. Rev. B* **2006**, *74*, 155108.
(36) Barzilai, S.; Halevy, I.; Yeheskel, O. Bulk modulus of Sc_2O_3: Ab initio calculations and experimental results. *J. Appl. Phys.* **2011**, *110*, 043532.
(37) Nishio-Hamane, D.; Katagiri, M.; Niwa, K.; Sano-Furukawa, A.; Okada, T.; Yagi, T. A new high-pressure polymorph of Ti_2O_3: implication for high-pressure phase transition in sesquioxides. *High Press. Res.* **2009**, *29*, 379−388.
(38) Wachtman, J. B. J.; Tefft, W. E.; Lam, D. G. Elastic constants of rutile (TiO_2). *J. Res. Natl. Bur. Stand., Sect. A* **1962**, *66A*, 465.
(39) Al-Khatatbeh, Y.; Lee, K. K. M.; Kiefer, B. High-pressure behavior of TiO_2 as determined by experiment and theory. *Phys. Rev. B* **2009**, *79*, 134114.
(40) Swamy, V.; Dubrovinsky, L. Bulk modulus of anatase. *J. Phys. Chem. Solids* **2001**, *62*, 673−675.
(41) Fu, Z.; Liang, Y.; Wang, S.; Zhong, Z. Structural phase transition and mechanical properties of TiO_2 under high pressure. *Phys. Status Solidi B* **2013**, *250*, 2206−2214.
(42) Wu, Y.; Zhang, Q.; Wu, X.; Qin, S.; Liu, J. High pressure structural study of β-Ti_3O_5: X-ray diffraction and Raman spectroscopy. *J. Solid State Chem.* **2012**, *192*, 356−359.
(43) Åsbrink, S.; Gerward, L.; Olsen, J. S. A high-pressure study of Ti_3O_5 by X-ray diffraction and synchrotron radiation. 1. Pressures up to 38.6 GPa. *J. Appl. Crystallogr.* **1989**, *22*, 119−122.
(44) Finger, L. W.; Hazen, R. M. Crystal structure and isothermal compression of Fe_2O_3, Cr_2O_3, and V_2O_3 to 50 kbars. *J. Appl. Phys.* **1980**, *51*, 5362−5367.
(45) Sato, Y.; Akimoto, S. Hydrostatic compression of four corundum-type compounds: α-Al_2O_3, V_2O_3, Cr_2O_3, and α-Fe_2O_3. *J. Appl. Phys.* **1979**, *50*, 5285−5291.
(46) Bai, L.; Li, Q.; Corr, S. A.; Pravica, M.; Chen, C.; Zhao, Y.; Sinogeikin, S. V.; Meng, Y.; Park, C.; Shen, G. Pressure-induced cation-cation bonding in V_2O_3. *Phys. Rev. B* **2015**, *92*, 134106.
(47) Li, Q.; Zhang, H.; Lin, C.; Tian, F.; Smith, J. S.; Park, C.; Liu, B.; Shen, G. Pressure-induced phase transitions and insulator-metal transitions in VO_2 nanoparticles. *J. Alloys Compd.* **2017**, *709*, 260−266.
(48) Bai, L.; Li, Q.; Corr, S. A.; Meng, Y.; Park, C.; Sinogeikin, S. V.; Ko, C.; Wu, J.; Shen, G. Pressure-induced phase transitions and metallization in VO_2. *Phys. Rev. B* **2015**, *91*, 104110.
(49) Dymshits, A. M.; Dorogokupets, P. I.; Sharygin, I. S.; Litasov, K. D.; Shatskiy, A.; Rashchenko, S. V.; Ohtani, E.; Suzuki, A.; Higo, Y. Thermoelastic properties of chromium oxide Cr_2O_3 (eskolaite) at high pressures and temperatures. *Phys. Chem. Miner.* **2016**, *43*, 447−458.
(50) Maddox, B. R.; Yoo, C. S.; Kasinathan, D.; Pickett, W. E.; Scalettar, R. T. High-pressure structure of half-metallic CrO_2. *Phys. Rev. B* **2006**, *73*, 144111.
(51) Jog, K. N.; Singh, R. K.; Sanyal, S. P. Phase transition and high-pressure behavior of divalent metal oxides. *Phys. Rev. B* **1985**, *31*, 6047−6057.
(52) Zhang, J. Room-temperature compressibilities of MnO and CdO: further examination of the role of cation type in bulk modulus systematics. *Phys. Chem. Miner.* **1999**, *26*, 644−648.
(53) Jeanloz, R.; Rudy, A. Static compression of MnO manganosite to 60 GPa. *J. Geophys. Res. Solid* **1987**, *92*, 11433−11436.
(54) Finger, L.; Hazen, R.; Hofmeister, A. High-Pressure crystal chemistry of spinel ($MgAl_2O_4$) and magnetite (Fe_3O_4): Comparisons with silicate spinels. *Phys. Chem. Miner.* **1986**, *13*, 215−220.
(55) Wilburn, D. R.; Bassett, W. A. Hydrostatic compression of iron and related compounds; an overview. *Am. Mineral.* **1978**, *63*, 591−596.
(56) Olsen, J.; Cousins, C.; Gerward, L.; Jhans, H.; Sheldon, B. A study of the crystal structure of Fe_2O_3 in the pressure range up to 65 GPa using synchrotron radiation. *Phys. Scr.* **1991**, *43*, 327.
(57) Ohnishi, S.; Mizutani, H. Crystal field effect on bulk moduli of transition metal oxides. *J. Geophys. Res.* **1978**, *83*, 1852−1856.
(58) Bai, L.; Pravica, M.; Zhao, Y.; Park, C.; Meng, Y.; Sinogeikin, S. V.; Shen, G. Charge transfer in spinel Co_3O_4 at high pressures. *J. Phys.: Condens. Matter* **2012**, *24*, 435401.
(59) Hirai, S.; Mao, W. L. Novel pressure-induced phase transitions in Co_3O_4. *Appl. Phys. Lett.* **2013**, *102*, 041912.
(60) Beg, M. M.; Shapiro, S. M. Study of phonon dispersion relations in cuprous oxide by inelastic neutron scattering. *Phys. Rev. B* **1976**, *13*, 1728−1734.

(61) Ehrenberg, H.; McAllister, J. A.; Marshall, W. G.; Attfield, J. P. Compressibility of copper-oxygen bonds: a high-pressure neutron powder diffraction study of CuO. *J. Phys.: Condens. Matter* **1999**, *11*, 6501−6508.
(62) Palko, J. W.; Kriven, W. M.; Sinogeikin, S. V.; Bass, J. D.; Sayir, A. Elastic constants of yttria (Y_2O_3) monocrystals to high temperatures. *J. Appl. Phys.* **2001**, *89*, 7791−7796.
(63) Chan, S.-K.; Fang, Y.; Grimsditch, M.; Li, Z.; Nevitt, M. V.; Robertson, W. M.; Zouboulis, E. S. Temperature Dependence of the Elastic Moduli of Monoclinic Zirconia. *J. Am. Ceram. Soc.* **1991**, *74*, 1742−1744.
(64) Kisi, E. H.; Howard, C. J. Elastic Constants of Tetragonal Zirconia Measured by a New Powder Diffraction Technique. *J. Am. Ceram. Soc.* **1998**, *81*, 1682−1684.
(65) Boyle, W. F.; Bennett, J. G.; Shin, S. H.; Sladek, R. J. Elastic constants of NbO_2 at room temperature. *Phys. Rev. B* **1976**, *14*, 526−530.
(66) Wu, A. Y.; Sladek, R. J. Elastic constants of NbO_2 between 1.6 and 298 K. *Phys. Rev. B* **1982**, *26*, 2159−2167.
(67) Liu, D.; Lei, W. W.; Hao, J.; Liu, D. D.; Liu, B. B.; Wang, X.; Chen, X. H.; Cui, Q. L.; Zou, G. T.; Liu, J.; Jiang, S. High-pressure Raman scattering and x-ray diffraction of phase transitions in MoO_3. *J. Appl. Phys.* **2009**, *105*, 023513.
(68) Leger, J.-M.; Haines, J.; Blanzat, B. Materials potentially harder than diamond: Quenchable high-pressure phases of transition metal dioxides. *J. Mater. Sci. Lett.* **1994**, *13*, 1688−1690.
(69) Hazen, R. M.; Finger, L. W. Bulk moduli and high-pressure crystal structures of rutile-type compounds. *J. Phys. Chem. Solids* **1981**, *42*, 143−151.
(70) Christy, A. G.; Clark, S. M. Structural behavior of palladium (II) oxide and a palladium suboxide at high pressure: An energy-dispersive x-ray-diffraction study. *Phys. Rev. B* **1995**, *52*, 9259−9265.
(71) Liu, H.; Mao, H.-K.; Somayazulu, M.; Ding, Y.; Meng, Y.; Häusermann, D. *B*1-to-*B*2 phase transition of transition-metal monoxide CdO under strong compression. *Phys. Rev. B* **2004**, *70*, 094114.
(72) Jayaraman, A.; Wang, S. Y.; Sharma, S. K.; Ming, L. C. Pressure-induced phase transformations in HfO_2 to 50 GPa studied by Raman spectroscopy. *Phys. Rev. B* **1993**, *48*, 9205−9211.
(73) Leger, J. M.; Atouf, A.; Tomaszewski, P. E.; Pereira, A. S. Pressure-induced phase transitions and volume changes in HfO_2 up to 50 GPa. *Phys. Rev. B* **1993**, *48*, 93−98.
(74) Tsuda, N.; Sumino, Y.; Ohno, I.; Akahane, T. Elastic Constants of ReO_3. *J. Phys. Soc. Jpn.* **1976**, *41*, 1153−1158.
(75) Bolzan, A. A.; Fong, C.; Kennedy, B. J.; Howard, C. J. Structural Studies of Rutile-Type Metal Dioxides. *Acta Crystallogr. B* **1997**, *53*, 373−380.
(76) Rogers, D. B.; Shannon, R. D.; Sleight, A. W.; Gillson, J. L. Crystal chemistry of metal dioxides with rutile-related structures. *Inorg. Chem.* **1969**, *8*, 841−849.
(77) Demazeau, G.; Matar, S. F.; Pöttgen, R. Chemical Bonding in Metallic Rutile-type Oxides TO_2 (T = Ru, Rh, Pd, Pt). *Z. Naturforsch. B* **2007**, *62*, 949−954.
(78) Riga, J.; Tenret-Noël, C.; Pireaux, J. J.; Caudano, R.; Verbist, J. J.; Gobillon, Y. Electronic Structure of Rutile Oxides TiO_2, RuO_2 and IrO_2 Studied by X-ray Photoelectron Spectroscopy. *Phys. Scr.* **1977**, *16*, 351−354.
(79) Magneli, A.; Siitonen, S.; Skrifvars, B.; Schliack, J.; Reio, L. Studies on rhenium oxides. *Acta Chem. Scand.* **1957**, *11*, 28−33.
(80) Ivanovskii, A.; Chupakhina, T.; Zubkov, V.; Tyutyunnik, A.; Krasilnikov, V.; Bazuev, G.; Okatov, S.; Lichtenstein, A. Structure and electronic properties of new rutile-like rhenium (IV) dioxide ReO_2. *Phys. Lett. A* **2005**, *348*, 66−70.
(81) Werfel, F.; Brümmer, O. Corundum Structure Oxides Studied by XPS. *Phys. Scr.* **1983**, *28*, 92−96.
(82) Grillo, M. E. Stability of corundum- versus rutile-type structures of ruthenium and rhodium oxides. *Phys. Rev. B* **2004**, *70*, 184115.
(83) Binks, J. H.; Duffy, J. A. Chemical bonding in rock salt structured transition metal oxides. *J. Solid State Chem.* **1990**, *87*, 195−201.
(84) Oliva, R.; Ibáñez, J.; Artús, L.; Cuscó, R.; Zúñiga-Pérez, J.; Muñoz-Sanjosé, V. High-pressure Raman scattering of CdO thin films grown by metal-organic vapor phase epitaxy. *J. Appl. Phys.* **2013**, *113*, 053514.
(85) Fadda, G.; Colombo, L.; Zanzotto, G. First-principles study of the structural and elastic properties of zirconia. *Phys. Rev. B* **2009**, *79*, 214102.
(86) Gopal, P.; Spaldin, N. Polarization, piezoelectric constants and elastic constants of ZnO, MgO, and CdO. *J. Electron. Mater.* **2006**, *35*, 538−542.
(87) Cortona, P.; Mebarki, M. Cu_2O behavior under pressure: an ab initio study. *J. Phys.: Condens. Matter* **2011**, *23*, 045502.
(88) Iuga, M.; Steinle-Neumann, G.; Meinhardt, J. Ab-initio simulation of elastic constants for some ceramic materials. *Eur. Phys. J. B* **2007**, *58*, 127−133.
(89) Birch, F. Elastic constants of rutile—A correction to a paper by R. K. Verma, "Elasticity of some high-density crystals". *J. Geophys. Res.* **1960**, *65*, 3855−3856.
(90) Vick, G. L.; Hollander, L. E. Ultrasonic measurement of the elastic moduli of rutile. *J. Acoust. Soc. Am.* **1960**, *32*, 947−949.
(91) Labat, F.; Baranek, P.; Domain, C.; Minot, C.; Adamo, C. Density functional theory analysis of the structural and electronic properties of TiO_2 rutile and anatase polytypes: Performances of different exchange-correlation functionals. *J. Chem. Phys.* **2007**, *126*, 154703.
(92) Mouhat, F.; Coudert, F.-X. Necessary and sufficient elastic stability conditions in various crystal systems. *Phys. Rev. B* **2014**, *90*, 224104.
(93) Py-Renaudie, A.; Daoust, P.; Côté, M.; Desjardins, P.; Masut, R. A. Ab initio piezoelectric properties of wurtzite ZnO-based alloys: Impact of the *c*/*a* cell ratio. *Phys. Rev. Materials* **2020**, *4*, 053601.
(94) Mickevicius, V. V.; Burlys, R. P.; Sirvaitis, A. Y.; Griskevicius, D. S. *Litov. Fiz. Sb.* **1985**, *25*, 56.
(95) Carlotti, G.; Fioretto, D.; Socino, G.; Verona, E. Brillouin scattering determination of the whole set of elastic constants of a single transparent film of hexagonal symmetry. *J. Phys.: Condens. Matter* **1995**, *7*, 9147−9153.
(96) Nakamura, K.; Higuchi, S.; Ohnuma, T. Enhancement of piezoelectric constants induced by cation-substitution and two-dimensional strain effects on ZnO predicted by density functional perturbation theory. *J. Appl. Phys.* **2016**, *119*, 114102.
(97) Nevitt, M.; Chan, S.-K.; Liu, J.; Grimsditch, M.; Fang, Y. The elastic properties of monoclinic ZrO_2. *Physica B* **1988**, *150*, 230−233.
(98) Uchida, N.; Saito, S. Elastic Elastic Constants and Acoustic Absorption Coefficients in MnO, CoO, and NiO Single Crystals at Room Temperature. *J. Acoust. Soc. Am.* **1972**, *51*, 1602−1605.
(99) Tasnádi, F.; Odén, M.; Abrikosov, I. A. Ab initio elastic tensor of cubic $Ti_{0.5}Al_{0.5}N$ alloys: Dependence of elastic constants on size and shape of the supercell model and their convergence. *Phys. Rev. B* **2012**, *85*, 144112.
(100) Mozafari, E.; Shulumba, N.; Steneteg, P.; Alling, B.; Abrikosov, I. A. Finite-temperature elastic constants of paramagnetic materials within the disordered local moment picture from ab initio molecular dynamics calculations. *Phys. Rev. B* **2016**, *94*, 054111.
(101) Pitike, K. C.; Marquez-Rossy, A. E.; Flores-Betancourt, A.; Chen, D. X.; Santosh, K.; Cooper, V. R.; Lara-Curzio, E. On the elastic anisotropy of the entropy-stabilized oxide (Mg, Co, Ni, Cu, Zn)O compound. *J. Appl. Phys.* **2020**, *128*, 015101.
(102) Oliver, D. W. The Elastic Moduli of MnO. *J. Appl. Phys.* **1969**, *40*, 893−893.
(103) Plessis, P d. V D.; Tonder, S J v.; Alberts, L Elastic constants of a NiO single crystal: I (Magnetic transitions). *J. Phys. C: Solid State Phys.* **1971**, *4*, 1983−1987.
(104) Manghnani, M. H.; Brower, W. S.; Parker, H. S. Anomalous elastic behavior in Cu_2O under pressure. *Phys. Status Solidi A* **1974**, *25*, 69−76.

https://doi.org/10.1021/acs.cgd.2c01543
Cryst. Growth Des. 2023, 23, 3427−3436

(105) Steneteg, P.; Hellman, O.; Vekilova, O. Y.; Shulumba, N.; Tasnádi, F.; Abrikosov, I. A. Temperature dependence of TiN elastic constants from ab initio molecular dynamics simulations. *Phys. Rev. B* **2013**, *87*, 094114.
(106) Råsander, M.; Moram, M. A. On the accuracy of commonly used density functional approximations in determining the elastic constants of insulators and semiconductors. *J. Chem. Phys.* **2015**, *143*, 144104.

https://doi.org/10.1021/acs.cgd.2c01543
Cryst. Growth Des. 2023, 23, 3427−3436